THE JOURNAL OF PHYSICAL CHEMISTRY C
A JOURNAL OF THE AMERICAN CHEMICAL SOCIETY

pubs.acs.org/JPCC

Article

Magnetic Particle Spectroscopy with One-Stage Lock-In Implementation for Magnetic Bioassays with Improved Sensitivities

Vinit Kumar Chugh,[⊥] Kai Wu,*[,⊥] Venkatramana D. Krishna, Arturo di Girolamo, Robert P. Bloom, Yongqiang Andrew Wang, Renata Saha, Shuang Liang, Maxim C-J Cheeran,* and Jian-Ping Wang*

Cite This: *J. Phys. Chem. C* 2021, 125, 17221−17231

Read Online

ACCESS | Metrics & More | Article Recommendations | Supporting Information

ABSTRACT: In recent years, magnetic particle spectroscopy (MPS) has become a highly sensitive and versatile sensing technique for quantitative bioassays. It relies on the dynamic magnetic responses of magnetic nanoparticles (MNPs) for the detection of target analytes in the liquid phase. There are many research studies reporting the application of MPS for detecting a variety of analytes including viruses, toxins, nucleic acids, and so forth. Herein, we report a modified version of the MPS platform with the addition of a one-stage lock-in design to remove the feedthrough signals induced by external driving magnetic fields, thus capturing only MNP responses for improved system sensitivity. This one-stage lock-in MPS system is able to detect as low as 781 ng multi-core Nanomag50 iron oxide MNPs (micromod Partikeltechnologie GmbH) and 78 ng single-core SHB30 iron oxide MNPs (Ocean NanoTech). We first demonstrated the performance of this MPS system for bioassay-related applications. Using the SARS-CoV-2 spike protein as a model, we have achieved a detection limit of 125 nM (equal to 5 pmole) for detecting spike protein molecules in the liquid phase. In addition, using a streptavidin−biotin binding system as a proof-of-concept, we show that these single-core SHB30 MNPs can be used for Brownian relaxation-based bioassays while the multi-core Nanomag50 cannot be used. The effects of MNP amount on the concentration-dependent response profiles for detecting streptavidin were also investigated. Results show that by using a lower concentration/amount of MNPs, concentration−response curves shift to a lower concentration/amount of target analytes. This lower concentration−response indicates the possibility of improved bioassay sensitivities by using lower amounts of MNPs.

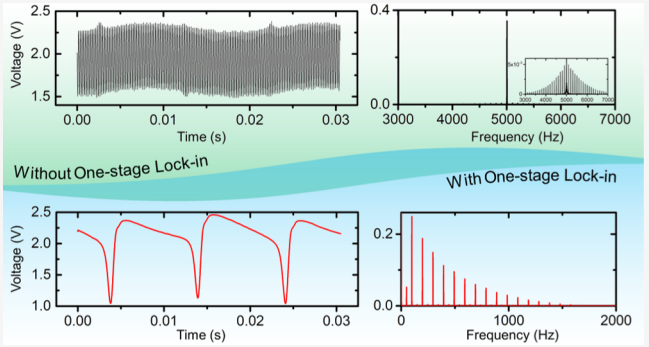

1. INTRODUCTION

Magnetic particle spectroscopy (MPS) for magnetic bioassays was first reported in 2006.[1,2] It is a technology derived from magnetic particle imaging, which relies on the nonlinear magnetization curves of magnetic nanoparticle (MNP) tracers for medical tomographic imaging.[3] However, on the other hand, MPS monitors the dynamic magnetic responses of MNPs in the liquid phase and assists in the analysis of the nanoparticles' binding status. To be specific, MNPs dispersed in a liquid add an additional degree of rotational freedom that allows for bioassays directly from the liquid phase. Upon the application of external AC magnetic fields (also called driving fields or excitation fields), the magnetizations of MNPs follow the field direction through a Brownian relaxation process, which is a physical rotational motion of nanoparticles. The dynamic magnetic responses of MNPs can be transformed to real-time voltage signals and monitored by using a pair of pick-up coils. The signal spectrum contains higher harmonics that are uniquely generated by MNPs. MPS-based bioassays use these harmonics of oscillating MNPs as a measure of the rotational freedom, that is, the bound status of MNPs, to target analytes from the liquid phase. With appropriate chemical modifications, MNPs can be surface-functionalized with proteins (such as antibodies, antigens, streptavidin, biotin, etc.), nucleic acids (DNA and RNA), and polymers, customized according to different bioassay purposes.[4−6] These surface-functionalized MNPs are nanoprobes that can bind to target analytes with high specificity and have shown great promise not only for MPS-based bioassays but also other magnetic bioassays including magnetoresistive and magnetic impedance biosensors and nuclear magnetic resonance biosensors.[7−17] In liquid phase MPS-based bioassays, the binding of MNPs to target analytes will hinder or even block the Brownian relaxation of MNPs and thus causes a phase lag between their magnetizations and the external AC magnetic

Received: June 10, 2021
Revised: July 20, 2021
Published: July 30, 2021

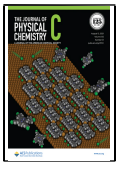

https://doi.org/10.1021/acs.jpcc.1c05126
J. Phys. Chem. C 2021, 125, 17221−17231

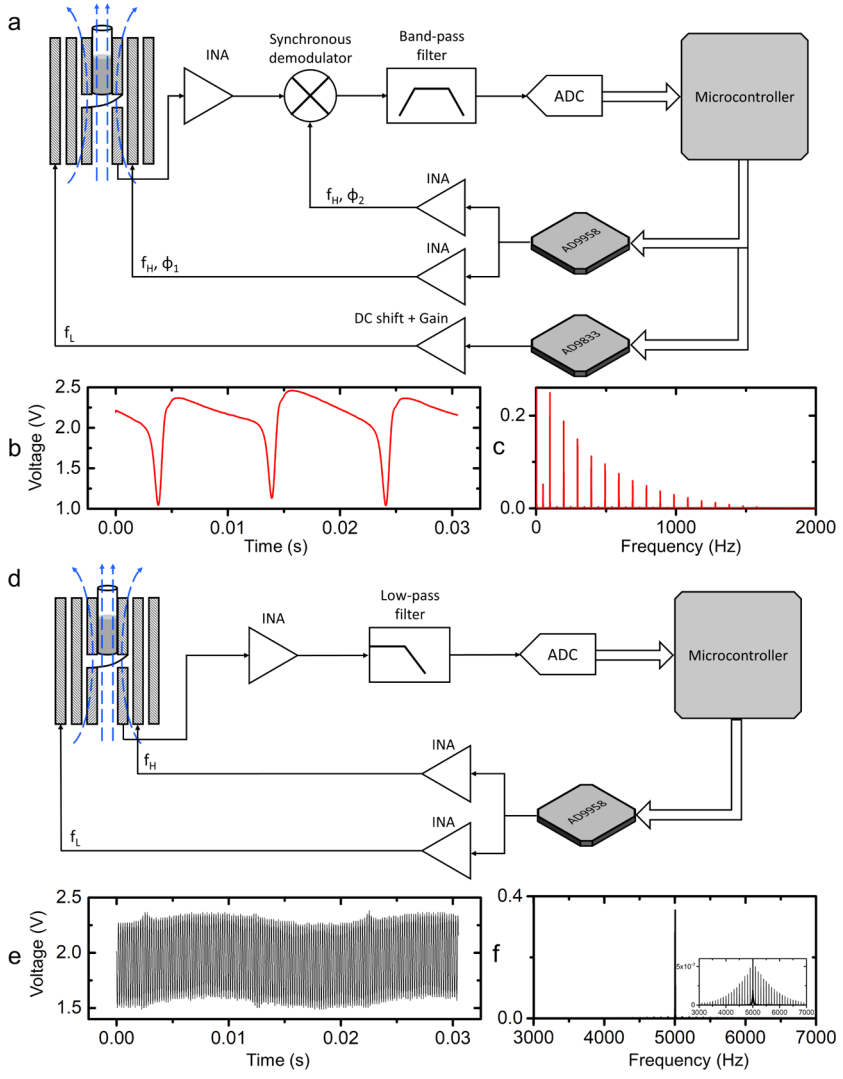

Figure 1. Schematic view of the MPS signal flow with (a) and without the (d) one-stage lock-in implementation. The temporal-domain signal as sampled by an ADC is shown in (b,e) while a corresponding signal depiction in the frequency domain is shown in (c,f) for the lock-in and without lock-in-based approaches.

fields[18] and a reduced AC magnetic susceptibility.[19] The binding of MNPs to analytes causes weaker dynamic magnetic responses of MNPs and, as a result, the harmonic amplitudes drop is expected. Thus, this assay mechanism allows for development of one-step, wash-free, and quantitative detection of target analytes directly in the liquid phase.[20,21]

In the past decade, various MPS platform designs have been reported, such as two-AC (also called frequency mixing) and one-AC driving field methods based on how the excitation fields are applied and the surface- and liquid phase-based bioassays (based on how the MNPs are bound).[11,12,20,22−28] However, a common issue with all MPS systems is the presence of feedthrough signal corresponding to the driving magnetic fields, which can be orders of magnitude higher than the MNP signal and can be a limiting factor in the MPS-based bioassays. Modalities based on both active and passive cancellations for such signals have been explored.[29−33] In the present work, we report a modified version of a two-AC magnetic field-based MPS system with the addition of a one-stage lock-in scheme for passive cancellation of the feedthrough signal and improved detection sensitivity. The performance and sensitivity of this one-stage lock-in MPS system is first evaluated by determining the lowest amount of MNPs detectable in the liquid phase. Then, we applied it to the detection of SARS-CoV-2 spike protein molecules, exploiting the Brownian-relaxation of MNPs. Finally, we explored the impact of MNP amounts on the ability of the MPS system to detect varied concentrations of target analytes by using a streptavidin−biotin binding system in the liquid phase.

2. MATERIALS AND METHODS

2.1. Materials. The Nanomag50 MNPs are 50 nm superparamagnetic dextran iron oxide composite nanoparticles functionalized with biotin, with a weight concentration of 5 mg/mL and a particle concentration of 91.36 nM, purchased from micromod Partikeltechnologie GmbH (product no. 79-26-501). The SHB30 MNPs are 30 nm iron oxide nanoparticles functionalized with biotin, with a weight concentration of 1 mg/mL and a particle concentration of 34 nM, provided by Ocean NanoTech. Streptavidin from *Streptomyces avidinii* is purchased from Sigma-Aldrich (product no. S4762). The IPG30 MNPs are 30 nm iron oxide nanoparticles functionalized with protein G, with a weight concentration of

https://doi.org/10.1021/acs.jpcc.1c05126
J. Phys. Chem. C 2021, 125, 17221−17231

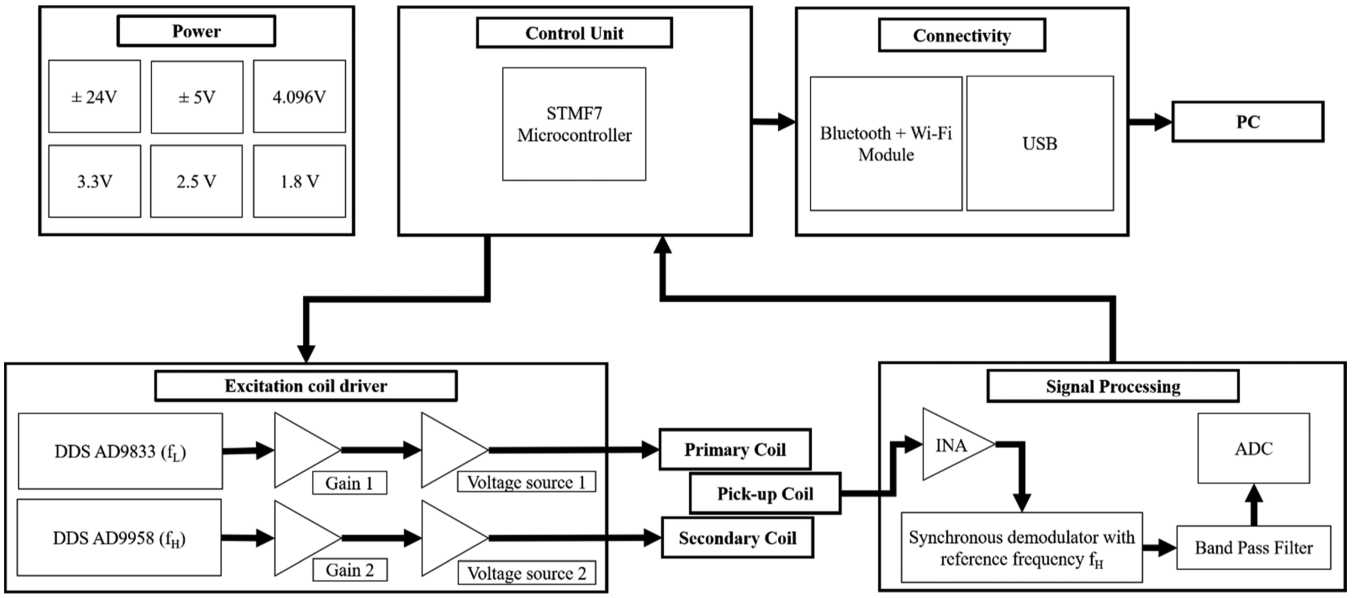

Figure 2. Block diagram of the MPS system with one-stage lock-in implementation.

1.7 mg/mL and a particle concentration of 57.8 nM, provided by Ocean NanoTech. The PS500-SV beads are 500 nm polystyrene beads coated with streptavidin purchased from Nanocs Inc. (product no. PS500-SV-1). The biotinylated spike protein [receptor-binding domain (RBD), His tag, consisting of 234 amino acids with a molecular mass of 26.54 kDa, product no. 40592-V08H-B] and the spike RBD antibody (polyclonal rabbit IgG, product no. 40592-T62) are purchased from Sino Biological Inc.

2.2. Magnetic Property Characterization. 10 μL of Nanomag50 and SH30 MNP suspensions are each transferred to a filter paper and air-dried. Then, the static magnetic hysteresis loops are measured by a physical properties measurement system (Quantum Design Inc.) to obtain the magnetic properties of these nanoparticles such as the saturation magnetization (M_s) and coercivity (H_c). The specific magnetic magnetizations (M, emu/g) of Nanomag50 and SHB30 MNPs under a 500 Oe field are 18.2 and 29.2 emu/g, respectively. Nanomag50 MNPs show superparamagnetic properties with zero magnetic coercivity, while, on the other hand, SHB30 MNPs show a coercivity field of 36 Oe. The hysteresis loops and magnetic properties of Nanomag50 and SHB30 MNPs are summarized in Supporting Information S1.

2.3. MPS Measurements. The dynamic magnetic responses of MNPs are characterized using a homebuilt one-stage lock-in MPS system. A fixed volume of MNP suspension (with or without protein analytes) is added to a glass vial that can fit into the pick-up coils. AC magnetic fields are applied by drive coils and the dynamic magnetic responses are sensed by pick-up coils in the form of a real-time voltage signal. Several MPS readings are taken from each vial and each reading consists of 170k discrete-time voltage samples from which the higher harmonics are extracted.

3. RESULTS AND DISCUSSION

3.1. MPS Platform. The MPS platform consists of two main parts, namely, magnetic field generation and MNP signal decoding. The MPS system operates on the frequency mixing modality where a magnetic field consisting of one high frequency (f_H) and one low frequency (f_L) components is applied and the dynamic magnetic response of the MNPs is recorded in accordance with the principle of Faraday's law. The experiments in this present work are conducted with the dual-frequency magnetic field having sinusoidal components of 5 KHz, 25 Oe for the high-frequency driving field and 50 Hz, 250 Oe for the low-frequency driving field. A balanced set of pick-up coils is used as shown in Figure 1a for recording the magnetic response, which in principle cancels out any electromagnetic field (EMF) generated due to the applied magnetic field and permits exclusive recording of the magnetic response from MNPs. However, in practice, the feedthrough signal (i.e., EMF due to driving fields) tends to be a real problem. Figure 1f shows the fast Fourier transform spectrum of the MNP response and it can be clearly observed that the feedthrough signal corresponding to f_H is 2 orders of magnitude higher than the 3rd harmonic responses of MNPs.

Herein, a one-stage lock-in-based approach is used to remove the feedthrough signals corresponding to driving field frequencies and to capture only the MNP responses. Figure 1a,d depicts schematic diagrams of the signal decoding topology with and without the one-stage lock-in implementation and the corresponding captured signals in temporal and frequency domains (Figure 1b,c,e,f). From Figure 1c, we can clearly observe that the one-stage lock-in approach significantly removes the feedthrough signals. Another advantage that the lock-in-based approach provides is the reduction of the sampling frequency requirements. Experiments on an MPS system without lock-in design (Figure 1d) require a sampling frequency of up to 500 KSPS to obtain optimal signal-to-noise ratio (SNR) performance. However, the lock-in-based approach shifts the MNP spectra to a lower frequency range and hence allows for better SNR performance with a lower sampling rate (100 KSPS) that is easily adaptable on a handheld system setting.

3.2. Circuit Design of a One-Stage Lock-In MPS System. The circuit for the one-stage lock-in MPS system can be divided into three main parts: (1) power, (2) excitation coil driver, and (3) signal processing. Figure 2 depicts a simplified

https://doi.org/10.1021/acs.jpcc.1c05126
J. Phys. Chem. C 2021, 125, 17221−17231

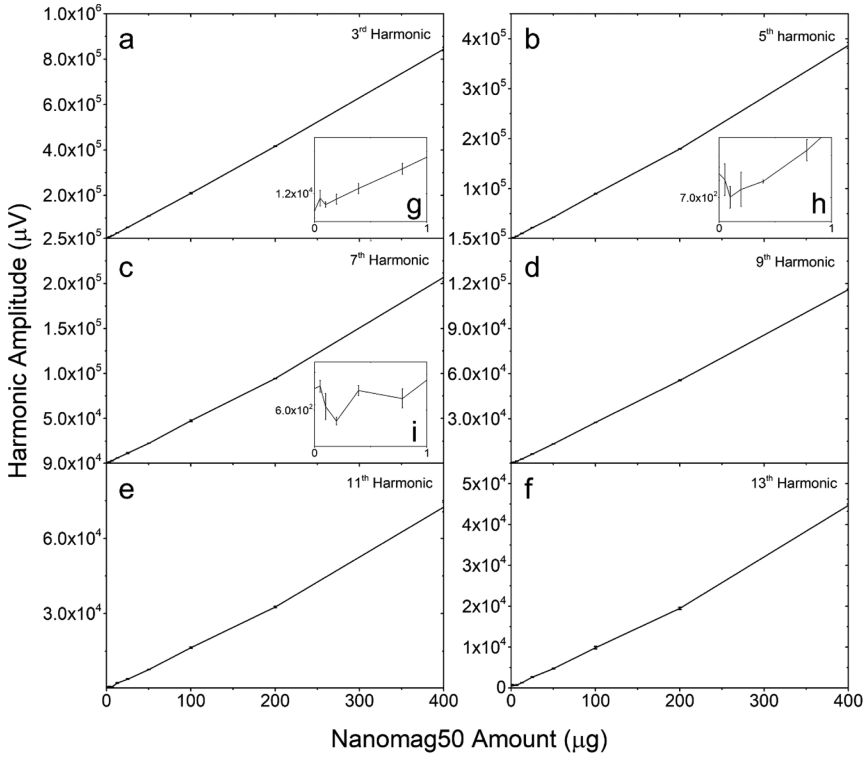

Figure 3. (a) 3rd, (b) 5th, (c) 7th, (d) 9th, (e) 11th, and (f) 13th harmonics collected from varying amounts of Nanomag50 MNPs. (g–i) zoomed-in views of the 3rd, 5th, and 7th harmonics collected from samples with the MNP amount below 1 μg per vial. Error bars represent standard errors. The minimum detectable amount of Nanomag50 MNPs is determined when the amplitude of the 3rd harmonic is at least twice the standard error higher than the 3rd harmonic amplitude of the blank sample. Herein, the minimum detectable amount of Nanomag50 MNPs is determined to be 781 ng.

block diagram of the one-stage lock-in MPS system developed for this work.

3.3. Power Generation. An MPS device requires different line voltages for operation of different system blocks. Briefly, the system requires ±24 V for the excitation coil voltage source driver, ±5 V for the signal processing stages, 3.3 V for AD9833 and STMF7 microcontrollers, 4.096 and 2.5 V for the analog to digital converter (ADC) reference and power correspondingly, and 1.8 V for the AD9958 DDS IC. The MPS device utilizes a 48 V wall adapter, GSM160A48-R7B (MEAN WELL Enterprises), as the main power source. The ±24 V supply is generated using a low-noise powerline split implementation using OPA549 (Texas Instruments), see Supporting Information S2 for details. The voltages 5, −5, 3.3, 2.5, and 1.8 V are generated using LDOs LT1117 (Linear Technology), LT1175 (Linear Technology), TPS62177 (Texas Instruments), ADP1715-2.5 (Analog Devices), and ADP3338-1.8 (Analog Devices), respectively.

3.4. Excitation Coil Driver. The coil excitation circuit consists of sine wave generation followed by voltage source implementation. A 2-channel DDS IC AD9958 (Analog Devices) is used for generation of sinusoids for a high-frequency (f_H) driving field and for phase-shifted reference to the synchronous demodulator in the signal processing stage. Differential output from AD9958 is passed through instrumentation amplifier INA128 (Texas Instruments) to convert into the single ended signal. DDS AD9833 (Analog Devices) is used for generation of sinusoid for a low-frequency (f_L) driving field. An inverting amplifier topology utilizing OPA548 (Texas Instruments) is used for the voltage source implementation for driving the primary and secondary coils.

3.5. Signal Processing. The differential signal from the pick-up coils is amplified using the precision instrumentation amplifier INA828 (Texas Instruments) for removing the common mode noise. The signal at this stage consists of the MNP response centered around a 5 KHz excitation frequency as can be seen in Figure 1f. The amplified signal is processed using a lock-in-based implementation consisting of an AD630 synchronous demodulator (Analog Devices) with a phase-shifted 5 KHz (f_H) reference signal followed by a band-pass filter to reject signal images at 0 Hz and around 10 KHz. The band-pass filter is implemented using the Sallen-key scheme. The filtered signal is sampled using LTC2368-24, 24-bit SAR ADC (Linear Technology, Analog Devices) at a 100 KSPS sampling rate. An STM32F747 microcontroller (STMicroelectronics) is used for handling and storing the sampled data, which are then transmitted to a PC using the UART communication protocol for further processing and analysis.

3.6. Minimum Detectable Amount of Nanomag50 and SHB30 MNPs by the One-Stage Lock-In MPS System. The sensitivity of our one-stage lock-in MPS system was first evaluated by assessing the minimum amount of MNPs detectable in the liquid phase. Briefly, two-fold dilutions of Nanomag50 and SHB30 MNP samples are prepared in glass vials and each vial contains 80 μL of the MNP suspension. Details of the experimental designs can be found in Supporting Information S3.

The Nanomag50 MNPs were diluted up to 8192 times, from 5 mg/mL (400 μg per vial, no dilution) to 610 ng/mL (48.8 ng per vial, 8192-fold dilution). Three independent MPS readings were carried out on each sample. As shown in Figure 3, the amplitudes of higher harmonics (i.e., from the 3rd to the

https://doi.org/10.1021/acs.jpcc.1c05126
J. Phys. Chem. C 2021, 125, 17221−17231

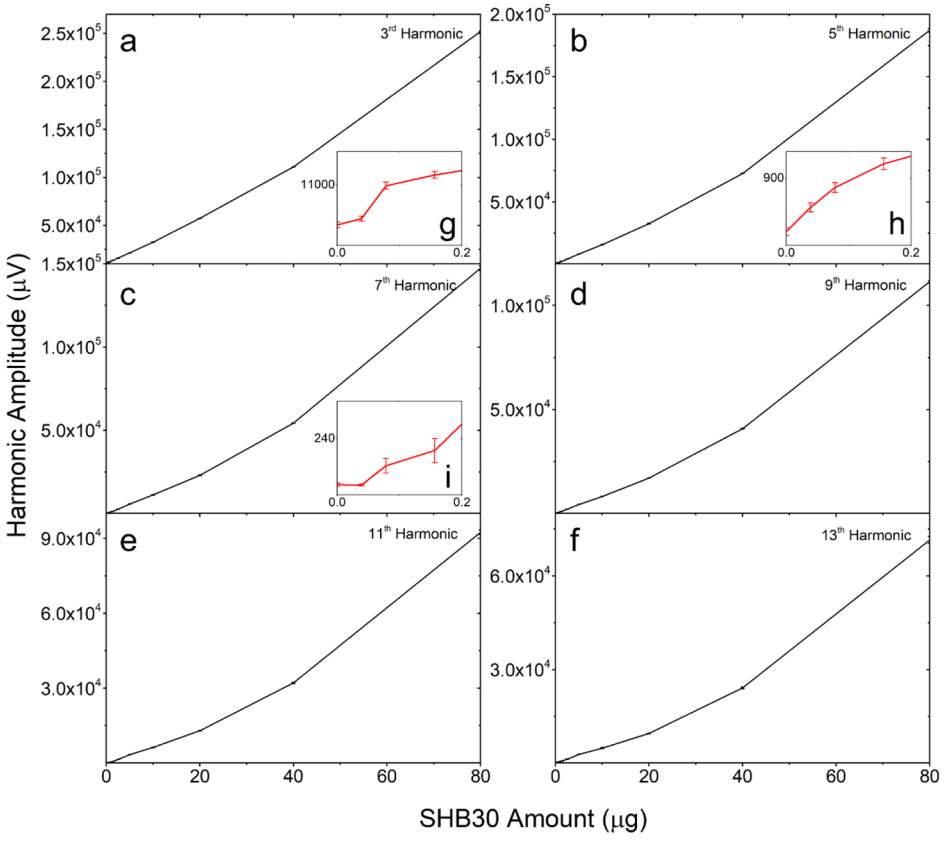

Figure 4. (a) 3rd, (b) 5th, (c) 7th, (d) 9th, (e) 11th, and (f) 13th harmonics collected from varying amounts of SHB30 MNPs. (g–i) enlarged views of the 3rd, 5th, and 7th harmonics collected from samples with the MNP amount below 200 ng per vial. Error bars represent standard error. The minimum detectable amount of SHB30 MNPs is determined to be 78 ng.

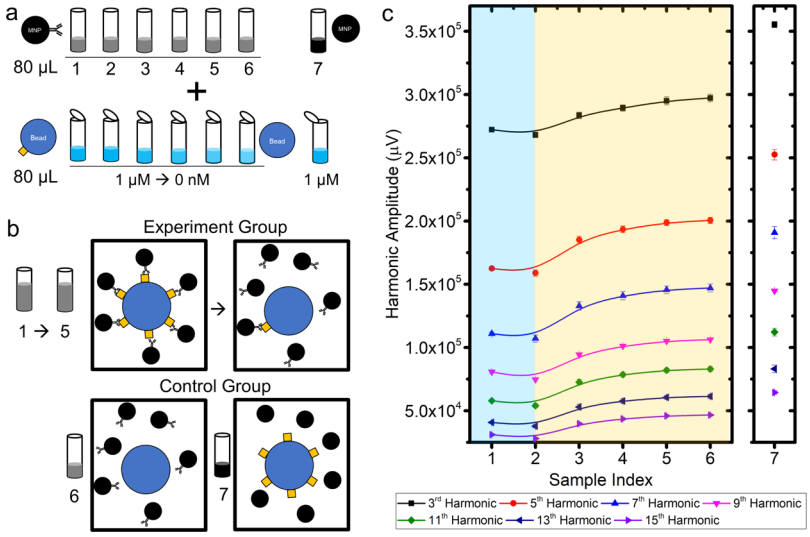

Figure 5. (a) Schematic view of the samples prepared for a one-step, wash-free, bead-based MPS bioassay for the detection of SARS-CoV-2 spike protein. (b) Schematic views of the MNP binding events for vials #1–7. (c) Concentration–response profiles for SARS-CoV-2 spike protein based on the 3rd to the 15th harmonics. Error bars represent standard errors.

13th harmonics in Figure 3a–f) linearly decreased as the amount of Nanomag50 MNPs decreases. The inset of Figure 3g shows a zoomed-in view of the 3rd harmonic amplitude collected from the lowest amount of Nanomag50 MNPs. The insets of Figure 3h,i are the zoomed-in views of the 5th and the 7th harmonic amplitudes collected from samples with lower MNP amounts. It was concluded that the minimum detectable amount of Nanomag50 MNPs by the MPS system is 781 ng (512-fold dilution).

In addition, varying amounts of SHB30 MNPs were prepared by twofold dilutions in the same manner. The SHB30 MNPs were diluted up to 2048 times, from 1 mg/mL (80 μg per vial, no dilution) to 488 ng/mL (39 ng per vial, 2048-fold dilution). As shown in Figure 4, the amplitude of the

https://doi.org/10.1021/acs.jpcc.1c05126
J. Phys. Chem. C 2021, 125, 17221–17231

Table 1. Experimental Designs for SARS-CoV-2 Spike Protein Detection

	MNP−Aby complex (80 μL per vial)		bead−protein complex (80 μL per vial)	
sample index	IPG30 MNP concentration/amount	spike RBD polyclonal antibody (pmole)	polystyrene beads (μL)	spike protein concentration/amount
#1	57.8 nM, 4.624 pmole	13.872	40	1 μM, 40 pmole
#2	57.8 nM, 4.624 pmole	13.872	40	500 nM, 20 pmole
#3	57.8 nM, 4.624 pmole	13.872	40	250 nM, 10 pmole
#4	57.8 nM, 4.624 pmole	13.872	40	125 nM, 5 pmole
#5	57.8 nM, 4.624 pmole	13.872	40	62.5 nM, 2.5 pmole
#6	57.8 nM, 4.624 pmole	13.872	40	0 nM, 0 pmole
#7	57.8 nM, 4.624 pmole	0	40	1 μM, 40 pmole

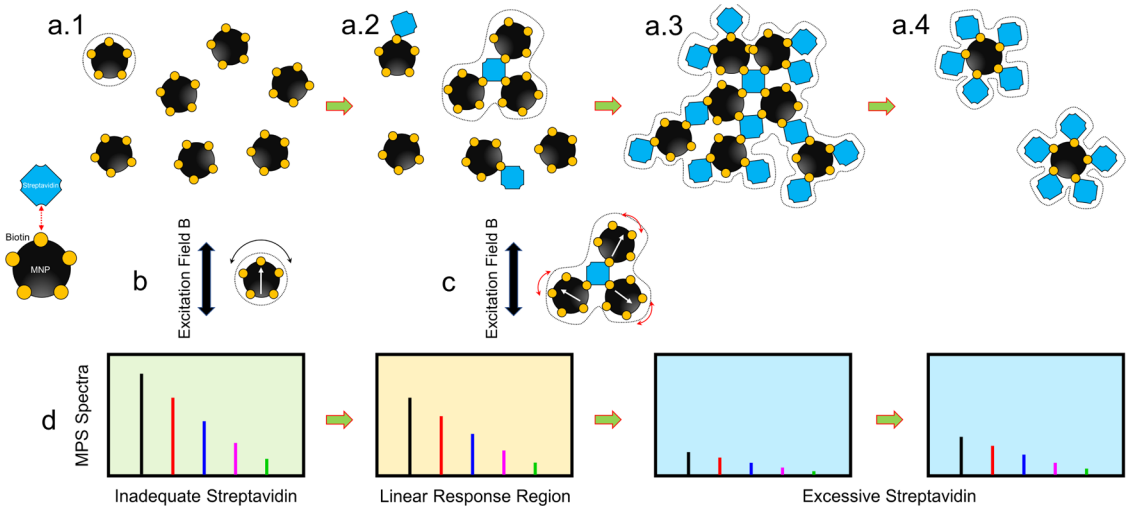

Figure 6. Streptavidin has a high binding affinity to biotin on the surface of SHB30 MNPs. With the addition of streptavidin as shown in (a), the MNPs form clusters and their Brownian relaxation process is blocked, (b,c). Under different scenarios with inadequate streptavidin, the linear response region, and excess streptavidin, the dynamic magnetic responses in the form of MPS spectra (higher harmonics from MNPs) become weaker, (d). Dashed closed loops depict the hydrodynamic sizes.

higher harmonic linearly decreases as the SHB30 amount decreases in the samples. The minimum detectable amount of SHB30 MNPs by the developed one-stage lock-in topology-based MPS system is 78 ng (1024-fold dilution). The modified MPS system shows a 50-fold improvement in sensitivity for detection of iron oxide MNPs when compared to our previous work (limit of detection was 4 μg) not utilizing a lock-in-based approach as shown in Figure 1d.[22]

3.7. One-Stage Lock-In MPS System for the Detection of SARS-CoV-2 Spike Protein. The performance of this one-stage lock-in MPS system was first verified by detecting SARS-CoV-2 spike protein molecules from PBS buffer. As shown in Figure 5a, seven samples were prepared and are listed in Table 1. Briefly, vials #1−6 each contained 80 μL of IPG30 MNPs that were surface-functionalized with SARS-CoV-2 spike RBD polyclonal antibody with MNP/Aby an ratio of 1:3. Vial #7 contained 80 μL of IPG30 without antibody functionalization, as a negative control sample. On the other hand, seven vials each containing 40 μL of 500 nm polystyrene beads (PS500-SV) mixed with 40 μL of biotinylated SARS-CoV-2 spike protein of varying concentrations from 0 nM to 1 μM were prepared. The biotinylated SARS-CoV-2 spike protein binds to streptavidin from beads and forms bead−protein complexes. The MNP−Aby complexes were then incubated with bead−protein complexes for 1 h to allow the specific antibody−antigen binding before MPS measurements. For the experimental group, namely, vials #1−5, MNPs bind to the polystyrene beads through antibody−antigen recognition, as shown in Figure 5b. As a result, this binding event blocks the Brownian relaxation of MNPs, thus causing a drop in the MPS spectra. However, for the negative control group, namely, vials #6 & 7, either spike protein molecules or polyclonal antibodies were missing.

The MPS spectra containing higher harmonics were collected from seven samples as summarized in Figure 5c. Vial #1 shows the scenario where excess amounts of spike protein molecules were present in the sample. Thus, the surface-functionalized MNPs may bind to free spike protein molecules instead of the fixed protein from polystyrene beads, forming small clusters. Although, these smaller MNP clusters will show weaker harmonic responses when compared to unbound MNPs, the harmonic response is still stronger than MNPs immobilized on the bead surface forming MNP−Aby−spike protein−bead complexes. The orange region in Figure 5c highlights the region of linear response where all the biotinylated spike protein molecules are conjugated with the streptavidin on the bead surface. Smaller spike protein concentrations lead to less MNPs binding to polystyrene beads and hence, we observe a smaller drop in MPS spectra for vials #2 through #6. As a negative control, we prepared vial #7 with MNPs that are not surface-conjugated with any antibodies. We observed the strongest harmonic response in this case as no MNP−polystyrene bead binding event takes place and the sample solution contains only of free-rotating MNPs. The detection limit for spike protein is determined from the vial where the amplitude of the 3rd harmonic is at

https://doi.org/10.1021/acs.jpcc.1c05126
J. Phys. Chem. C 2021, 125, 17221−17231

least twice the standard error higher than the 3rd harmonic amplitude of vial #6 (negative control). Based on this standard, the detection limit for SARS-CoV-2 spike protein was confirmed to be 125 nM (equal to 5 pmole).

3.8. Effect of MNP Amount on Analyte Concentration−Response Profiles. Herein, we explored the effect of MNP amount on concentration−response curves for analyte detection by using a streptavidin−biotin binding system. As shown in Figure 6, SHB30 MNPs were surface-functionalized with biotin molecules that have high binding affinity to streptavidin. When there is an inadequate amount (or lack of) of streptavidin to bind MNPs, as shown in Figure 6, MNPs can freely rotate through Brownian relaxation (Figure 6b) to align with driving magnetic fields, thus showing strong dynamic magnetic responses and large harmonic amplitudes (Figure 6c,d). With increasing amounts of streptavidin in the sample, MNPs form cluster matrices and exhibit larger hydrodynamic sizes (the closed loops in Figure 6). As a result, the clustered MNPs lose their rotational freedom and exhibit weaker dynamic magnetic responses to the driving fields and consequently lower harmonic amplitudes are expected (see Figure 6d). Based on the relative abundance of MNPs and streptavidin in the liquid sample, the degree of MNP clustering goes through the zone of inadequate analyte (a.1), linear response region (a.2), and zone of excessive analyte (a.3,a.4) as labeled in Figure 6. In the linear response region, the amounts of MNPs and streptavidin reach concentrations that enable formation of analyte−MNP cluster matrices. The formation of the matrix increases in a linear ratio until it exceeds an optimal concentration when the matrices dissociate, with excessive amounts of streptavidin. This MNP inter-linking continues along a linear scale until formation of large clusters of MNP−streptavidin completely blocks the Brownian relaxation of MNPs, resulting in the lowest harmonic amplitudes. As the concentration of streptavidin (analyte) increases, MNP−biotin binding sites will become saturated until they are fully occupied by streptavidin (see Figure 6a.4), the large cluster matrices are disrupted, and MNP clusters no longer form the majority in the liquid phase. Individual MNPs when saturated with streptavidin in this scenario will exhibit a harmonic response that is greater than that of large clusters but smaller than that of the free MNPs due to an increment in effective hydrodynamic size.

The goal of this experiment was to examine the effect of varying MNP amounts in the assay on the concentration−response profiles for detection of streptavidin in the liquid phase. Four experimental groups were designed, each consisting of 10 samples/vial and each vial containing 80 μL of SHB30 MNPs with the following concentration: (1) 8.5 nM (group I, particle amount: 680 fmole per vial, 4-fold dilution), (2) 4.25 nM (group II, particle amount: 340 fmole per vial, 8-fold dilution), (3) 2.125 nM (group III, particle amount: 170 fmole per vial, 16-fold dilution), and (4) 1.0625 nM (group IV, particle amount: 85 fmole per vial, 32-fold dilution). To all 10 vials from each group, 80 μL of varied streptavidin concentrations ranging from 400 to 0 nM were added, as shown in Table 2.

In short, 80 μL of SHB30 MNP suspensions of varying dilutions was mixed with 80 μL streptavidin of varying concentrations. The mixtures are incubated at room temperature for 30 min on a shaker to allow the binding of biotins on SHB30 MNPs to streptavidin in the liquid phase. MPS measurements are carried out on each vial and six independent MPS readings are taken from each sample.

Table 2. Experimental Designs for Groups I−IV

group no. sample index	SHB30 MNP concentration/amount (80 μL per vial)	streptavidin concentration/amount (80 μL per vial)
group I # 1−10	8.5 nM (4-fold dilution), 680 fmole	400 nM, 32 pmole (#1)
		300 nM, 24 pmole (#2)
group II # 1−10	4.25 nM (8-fold dilution), 340 fmole	200 nM, 16 pmole (#3)
		150 nM, 12 pmole (#4)
group III # 1−10	2.125 nM (16-fold dilution), 170 fmole	100 nM, 8 pmole (#5)
		50 nM, 4 pmole (#6)
group IV # 1−10	1.0625 nM (32-fold dilution), 85 fmole	25 nM, 2 pmole (#7)
		10 nM, 800 fmole (#8)
		5 nM, 400 fmole (#9)
		0 nM, 0 fmole (#10)

As shown in Figure 7a, clear concentration−response curves are observed from all four groups, the 3rd harmonics gradually decrease as the amount of streptavidin increases from vial #10 to #1. Vials #1 to #4 for group IV demonstrate the phenomena of MNP−biotin saturation with excess streptavidin, where most MNP-binding sites are fully occupied with streptavidin, decreasing the formation of large MNP clusters. This phenomenon is most apparent when higher 3rd and 5th harmonic signals were observed at higher analyte concentrations compared to vials #5−7 with lower streptavidin. It should also be noted that 3rd harmonic amplitude in vials #1−#4 (streptavidin saturation) was smaller than that of vials #9−10 (inadequate streptavidin case) where unbound MNPs form a majority in the liquid phase. For experimental groups I−III, the higher amount of streptavidin in vials #1−5 results in the clustering of SHB30 MNPs and hence lower harmonic signals are observed. As a result, this clustering hinders the Brownian relaxation of MNPs to realign their magnetic moments to the driving fields. As we reduce the streptavidin concentration/amount, it reaches to linear response region where the relative number of biotins from SHB30 MNPs is in the same order of magnitude as streptavidin. With further reduction of streptavidin concentration/amount, the harmonic signal increases and reaches a state where SHB30 MNPs can freely rotate following the driving magnetic fields since there is inadequate amount of streptavidin to enable MNP clustering and hinder their Brownian relaxation. We observed a weak reversal of harmonic signals from its nadir for groups I to III (in vials #1−4); however, the phenomenon was not as prominent as observed for group IV, even at the highest (400 nM) concentration of streptavidin tested. It is plausible that 400 nM streptavidin is insufficient to completely saturate MNP-associated biotins in groups I−III. These three different response zones are highlighted in blue (excessive amount of streptavidin), orange (linear response region), and green (inadequate streptavidin) regions in Figure 7e−h as well as in Figure 6d. Overall, the higher harmonics show parallel concentration−response curves in the 3rd harmonic signals. It is observed that the linear response region of concentration−response curve moves toward lower streptavidin quantities (as shown by the arrow in Figure 7a and summarized in Table 3) with the dilution of SHB30 MNPs from group I to group IV. Figure 7b−d compares the 3rd harmonic amplitudes of SHB30

https://doi.org/10.1021/acs.jpcc.1c05126
J. Phys. Chem. C 2021, 125, 17221−17231

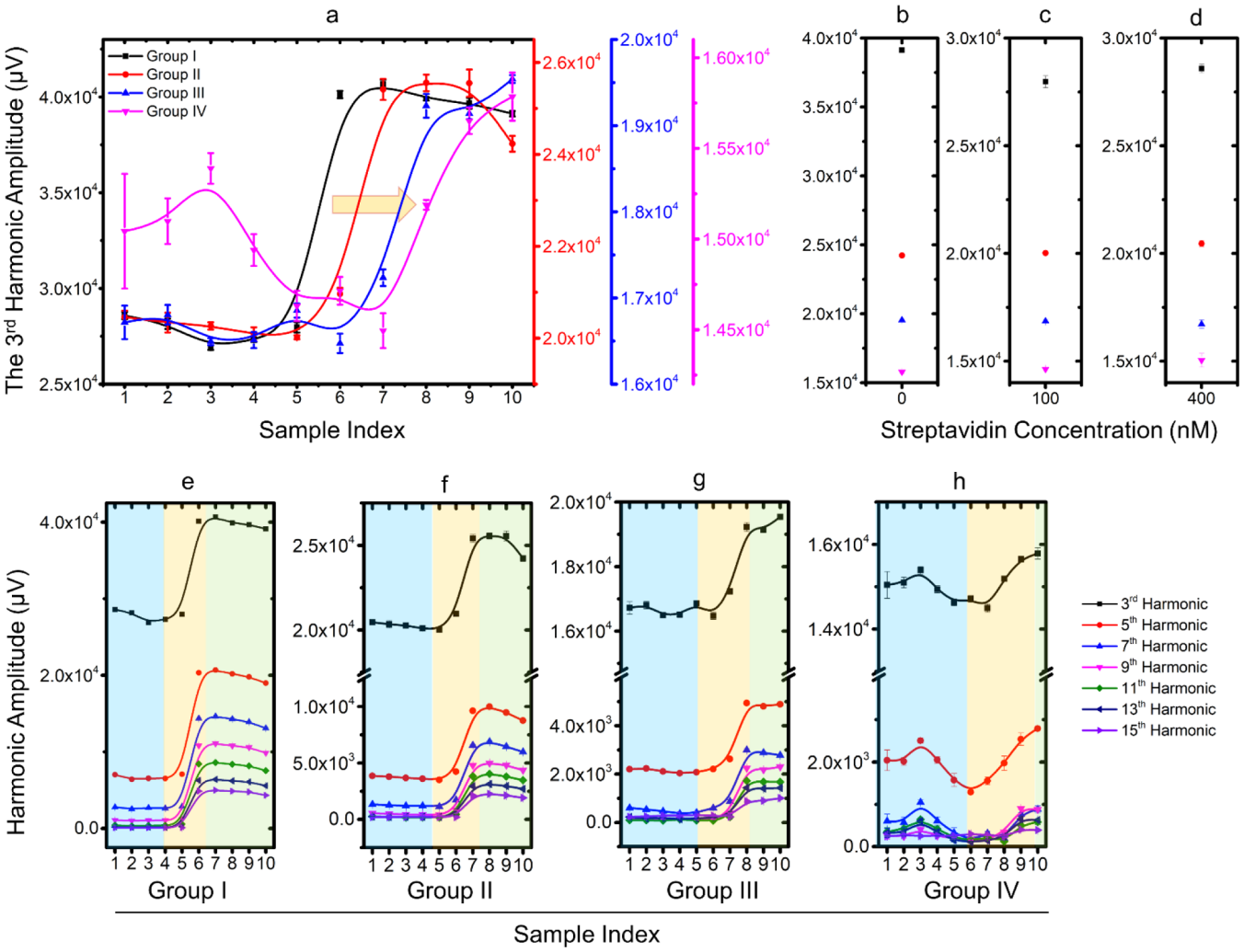

Figure 7. (a) Concentration−response profiles for streptavidin based on the 3rd harmonic amplitudes of SHB30 MNPs with 8.5 nM (group I, black), 4.25 nM (group II, red), 2.125 nM (group III, blue), and 1.0625 nM (group IV, magenta) concentrations. (b−d) 3rd harmonics of different dilutions of SHB30 MNPs mixed with 0, 100, and 400 nM streptavidin, respectively. (e−h) concentration−response profiles for streptavidin from groups I−IV based on the 3rd to the 15th harmonics. Error bars represent standard errors.

Table 3. Linear Response Region Observed from Concentration−Response Profiles Based on Different MNP Concentrations

group index	SHB30 MNP concentration (nM)	linear response region (streptavidin concentration) (nM)
I	8.5	50−100
II	4.25	25−100
III	2.125	10−50
IV	1.0625	5−25

MNPs from groups I−IV, detecting the same concentration/amount of streptavidin.

Interestingly, the best SNR performance was not observed from the 3rd harmonic response of the MNPs, but instead the least standard deviation was observed consistently when the 9th and 15th harmonics were used to represent MNP binding information. Figure 8a,b presents the concentration−response profiles for streptavidin based on the 9th and 15th harmonics, respectively. A plausible explanation for the observation could be the higher $1/f$ noise for the 3rd harmonic signal. During experiments, it was observed that the 3rd harmonic was more susceptible to surrounding noises. Most of these issues can be addressed by providing proper magnetic and EMI isolation to the system along with implementation of a second lock-in corresponding to the harmonic of interest to reject phase-separable noise.

The streptavidin−biotin binding experiments were also carried out on multi-core Nanomag50 MNPs, where each of the four experimental groups consists of 10 samples/vials was designed and each vial contained 80 μL of Nanomag50 MNP of 8.5, 4.25, 2.125, and 1.0625 nM concentrations. Due to the characteristic of the multi-core Nanomag50 MNPs having smaller superparamagnetic iron oxide nanoparticles embedded in the matrix, their Brownian relaxation is intrinsically blocked and hence, clustering does not impact their dynamic magnetic response. Thus, very weak or no harmonic signal changes were observed from Nanomag50 MNP samples mixed with varying concentrations/amounts of streptavidin. The experimental design and results of multi-core Nanomag50 MNP-based streptavidin tests are summarized in Supporting Information S4. The results indicate that multi-core MNPs, whose Brownian relaxation is intrinsically blocked, cannot be used for liquid-phase MPS-based bioassays.

https://doi.org/10.1021/acs.jpcc.1c05126
J. Phys. Chem. C 2021, 125, 17221−17231

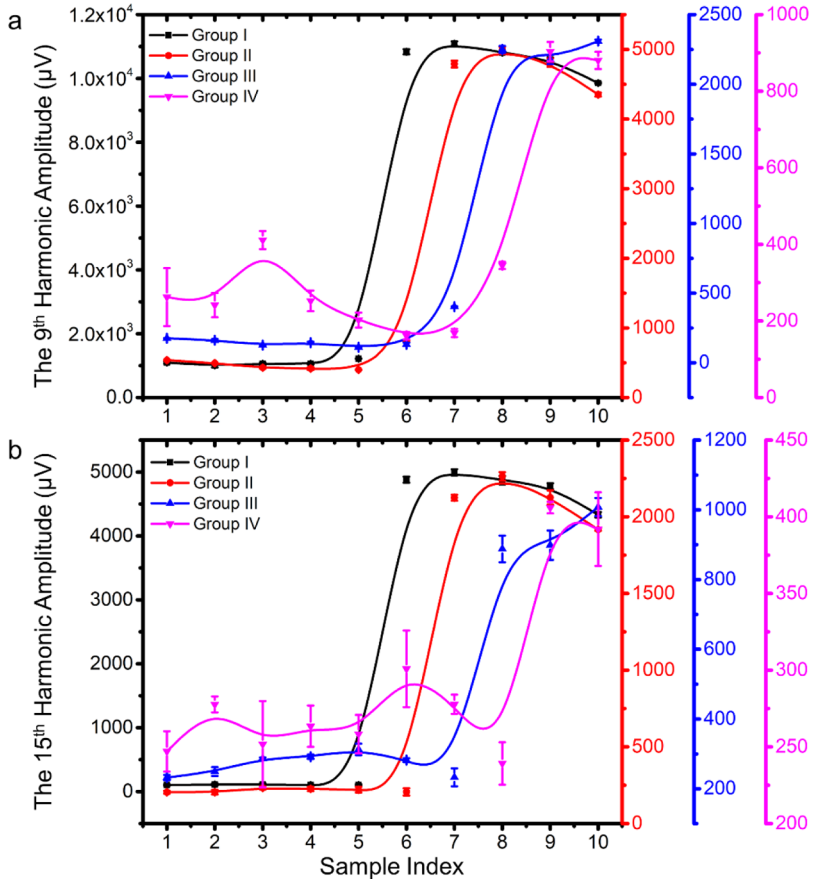

Figure 8. Concentration−response profiles for streptavidin based on the (a) 9th and (b) 15th harmonic amplitudes of SHB30 MNPs with 8.5 nM (group I, black), 4.25 nM (group II, red), 2.125 nM (group III, blue), and 1.0625 nM (group IV, magenta) concentrations. Error bars represent standard errors.

4. CONCLUSIONS AND FUTURE PROSPECTS

In the present study, we have reported a method for passive cancellation of feedthrough signal for dual-frequency (2 AC driving fields) MPS methodology. The sensitivity of this one-stage lock-in MPS system is first evaluated by detecting twofold dilutions of commercial iron oxide MNPs: SHB30 and Nanomag50. The lowest amount detectable by the system was confirmed to be 78 ng for the single-core SHB30 and 781 ng for the multi-core Nanomag50 iron oxide MNPs. As a proof-of-concept, we applied this MPS system to the detection of SARS-CoV-2 spike protein samples, where the MNPs were surface-functionalized with spike RBD polyclonal antibodies that can specifically bind to spike protein coated on polystyrene beads. The binding events fix MNPs to larger beads' surfaces, hence blocking their rotational freedom of motion. As a result, the dynamic magnetic responses of MNPs become weaker and harmonic amplitudes become lower. Using this bioassay strategy, we showed the minimum detectable amount of spike protein molecules on the MPS platform is 125 nM (equal to 5 pmole).

In addition, using a streptavidin−biotin binding system as a model, we explored the effects of MNP amount on concentration−responses profiles for detecting target analytes. By fine-tuning the MNP amount/concentration in the sample, we were able to shift the linear response region for streptavidin detection. Results confirmed that the liquid phase bioassay scheme shows improved sensitivity in our one-stage lock-in MPS system when a lower amount/concentration of MNPs is used. The linear response region shifts the detection ability to a lower concentration of streptavidin using lower MNP quantities. Using 8.5, 4.25, 2.125, and 1.0625 nM concentrations of MNPs for streptavidin detection, the linear response region shifts from 50−100, 25−100, and 10−50, down to 10−25 nM, respectively, pushing the detection limit of streptavidin further into the femtomole range. These concentration−response profiles indicate the possibility for improved bioassay sensitivities by using a lower amount/concentration of MNPs. In the present study, our one-stage lock-in MPS system is able to detect as low as 800 fmole of streptavidin using a 1.0625 nM concentration of MNPs. However, this detection limit can be further improved by using lower amounts (higher dilutions) of MNPs. In addition to improved sensitivities, the cost per assay can be further reduced by using a less amount of MNPs. Low-cost options allow the point-of-care assays to be available in impoverished regions with scarce medical resources.

Our future plans include improving the sensitivity of the MPS system by using active feedthrough cancellation techniques. The passive feedthrough cancellation reported in the present study helps remove the feedthrough signals before ADC sampling. Therefore, with proper amplifications in place, we can take advantage of true ADC resolution for improved sensitivity. However, this method of removing feedthrough signals and amplifying remnant signals still holds a disadvantage as the intrinsic noise components also get amplified through the amplification units. Active cancellation of feedthrough can help improve the signal-to-noise ratio

https://doi.org/10.1021/acs.jpcc.1c05126
J. Phys. Chem. C 2021, 125, 17221−17231

before the instrumentation amplifier stage and hence allow for better sensitivity in MPS bioassay applications. We believe this passive feedthrough cancellation methodology in the MPS system design and fine-tuning the MNP amount/concentration to shift the linear response region will elucidate new ways of increasing detection sensitivity of MPS-based bioassays.

■ ASSOCIATED CONTENT

Supporting Information

The Supporting Information is available free of charge at https://pubs.acs.org/doi/10.1021/acs.jpcc.1c05126.

Magnetic properties of Nanomag50 and SHB30 MNPs; low noise powerline split implementation; experimental designs for varying amounts of Nanomag50 and SHB30 MNPs; and multi-core Nanomag50 MNPs for streptavidin detection (PDF)

■ AUTHOR INFORMATION

Corresponding Authors

Kai Wu − *Department of Electrical and Computer Engineering, University of Minnesota, Minneapolis, Minnesota 55455, United States;* orcid.org/0000-0002-9444-6112; Email: wuxx0803@umn.edu

Maxim C-J Cheeran − *Department of Veterinary Population Medicine, University of Minnesota, St. Paul, Minnesota 55108, United States*; Email: cheeran@umn.edu

Jian-Ping Wang − *Department of Electrical and Computer Engineering, University of Minnesota, Minneapolis, Minnesota 55455, United States*; Email: jpwang@umn.edu

Authors

Vinit Kumar Chugh − *Department of Electrical and Computer Engineering, University of Minnesota, Minneapolis, Minnesota 55455, United States;* orcid.org/0000-0001-7818-7811

Venkatramana D. Krishna − *Department of Veterinary Population Medicine, University of Minnesota, St. Paul, Minnesota 55108, United States;* orcid.org/0000-0002-1980-5525

Arturo di Girolamo − *Department of Electrical and Computer Engineering, University of Minnesota, Minneapolis, Minnesota 55455, United States*

Robert P. Bloom − *Department of Electrical and Computer Engineering, University of Minnesota, Minneapolis, Minnesota 55455, United States*

Yongqiang Andrew Wang − *Ocean Nano Tech LLC, San Diego, California 92126, United States*

Renata Saha − *Department of Electrical and Computer Engineering, University of Minnesota, Minneapolis, Minnesota 55455, United States;* orcid.org/0000-0002-0389-0083

Shuang Liang − *Department of Chemical Engineering and Material Science, University of Minnesota, Minneapolis, Minnesota 55455, United States;* orcid.org/0000-0003-1491-2839

Complete contact information is available at: https://pubs.acs.org/10.1021/acs.jpcc.1c05126

Author Contributions

[⊥]V.K.C. and K.W. have contributed equally to this work.

Notes

The authors declare no competing financial interest.

■ ACKNOWLEDGMENTS

This study was financially supported by the Institute of Engineering in Medicine, the Robert F. Hartmann Endowed Chair professorship, the University of Minnesota Medical School, and the University of Minnesota Physicians and Fairview Health Services through a COVID-19 rapid response grant. This study was also financially supported by the U.S. Department of Agriculture−National Institute of Food and Agriculture (NIFA) under award number 2020-67021-31956. The research reported in this publication was supported by the National Institute of Dental & Craniofacial Research of the National Institutes of Health under award number R42DE030832. The content is solely the responsibility of the authors and does not necessarily represent the official views of the National Institutes of Health. Portions of this work were conducted in the Minnesota Nano Center, which is supported by the National Science Foundation through the National Nano Coordinated Infrastructure Network (NNCI) under award number ECCS-1542202.

■ REFERENCES

(1) Krause, H.-J.; Wolters, N.; Zhang, Y.; Offenhäusser, A.; Miethe, P.; Meyer, M. H. F.; Hartmann, M.; Keusgen, M. Magnetic Particle Detection by Frequency Mixing for Immunoassay Applications. *J. Magn. Magn. Mater.* **2007**, *311*, 436−444.

(2) Nikitin, P. I.; Vetoshko, P. M.; Ksenevich, T. I. New Type of Biosensor Based on Magnetic Nanoparticle Detection. *J. Magn. Magn. Mater.* **2007**, *311*, 445−449.

(3) Gleich, B.; Weizenecker, J. Tomographic Imaging Using the Nonlinear Response of Magnetic Particles. *Nature* **2005**, *435*, 1214−1217.

(4) Maleki, A.; Taheri-Ledari, R.; Soroushnejad, M. Surface Functionalization of Magnetic Nanoparticles via Palladium-catalyzed Diels-Alder Approach. *ChemistrySelect* **2018**, *3*, 13057−13062.

(5) Nosrati, H.; Salehiabar, M.; Davaran, S.; Ramazani, A.; Manjili, H. K.; Danafar, H. New Advances Strategies for Surface Functionalization of Iron Oxide Magnetic Nano Particles (IONPs). *Res. Chem. Intermed.* **2017**, *43*, 7423−7442.

(6) Wu, K.; Su, D.; Saha, R.; Wong, D.; Wang, J.-P. Magnetic Particle Spectroscopy-Based Bioassays: Methods, Applications, Advances, and Future Opportunities. *J. Phys. D: Appl. Phys.* **2019**, *52*, 173001.

(7) Su, D.; Wu, K.; Saha, R.; Peng, C.; Wang, J.-P. Advances in Magnetoresistive Biosensors. *Micromachines* **2020**, *11*, 34.

(8) Rizzi, G.; Lee, J.-R.; Guldberg, P.; Dufva, M.; Wang, S. X.; Hansen, M. F. Denaturation Strategies for Detection of Double Stranded PCR Products on GMR Magnetic Biosensor Array. *Biosens. Bioelectron.* **2017**, *93*, 155−160.

(9) Xianyu, Y.; Wang, Q.; Chen, Y. Magnetic Particles-Enabled Biosensors for Point-of-Care Testing. *Trac. Trends Anal. Chem.* **2018**, *106*, 213−224.

(10) Wang, T.; Zhou, Y.; Lei, C.; Luo, J.; Xie, S.; Pu, H. Magnetic Impedance Biosensor: A Review. *Biosens. Bioelectron.* **2017**, *90*, 418−435.

(11) Orlov, A. V.; Khodakova, J. A.; Nikitin, M. P.; Shepelyakovskaya, A. O.; Brovko, F. A.; Laman, A. G.; Grishin, E. V.; Nikitin, P. I. Magnetic Immunoassay for Detection of Staphylococcal Toxins in Complex Media. *Anal. Chem.* **2013**, *85*, 1154−1163.

(12) Wu, K.; Liu, J.; Saha, R.; Su, D.; Krishna, V. D.; Cheeran, M. C.-J.; Wang, J.-P. Magnetic Particle Spectroscopy for Detection of Influenza A Virus Subtype H1N1. *ACS Appl. Mater. Interfaces* **2020**, *12*, 13686−13697.

(13) Jeong, S.; Min, C.; Shao, H.; Castro, C. M.; Weissleder, R.; Lee, H. Miniaturized Nuclear Magnetic Resonance Platform for Rare Cell

Detection and Profiling. *Circulating Tumor Cells*; Springer New York, 2016; pp 183−200.
(14) Gee, M. S.; Ghazani, A. A.; Haq, R.; Wargo, J. A.; Sebas, M.; Sullivan, R. J.; Lee, H.; Weissleder, R. Point of Care Assessment of Melanoma Tumor Signaling and Metastatic Burden from MNMR Analysis of Tumor Fine Needle Aspirates and Peripheral Blood. *Nanomed. Nanotechnol. Biol. Med.* **2017**, *13*, 821−828.
(15) Dupré, A.; Lei, K.-M.; Mak, P.-I.; Martins, R. P.; Peng, W. K. Micro-and Nanofabrication NMR Technologies for Point-of-Care Medical Applications−A Review. *Microelectron. Eng.* **2019**, *209*, 66−74.
(16) Wu, K.; Klein, T.; Krishna, V. D.; Su, D.; Perez, A. M.; Wang, J.-P. Portable GMR Handheld Platform for the Detection of Influenza A Virus. *ACS Sens.* **2017**, *2*, 1594−1601.
(17) Blümich, B. Introduction to Compact NMR: A Review of Methods. *Trac. Trends Anal. Chem.* **2016**, *83*, 2−11.
(18) Tu, L.; Jing, Y.; Li, Y.; Wang, J.-P. Real-Time Measurement of Brownian Relaxation of Magnetic Nanoparticles by a Mixing-Frequency Method. *Appl. Phys. Lett.* **2011**, *98*, 213702.
(19) Chieh, J. J.; Yang, S. Y.; Jian, Z. F.; Wang, W. C.; Horng, H. E.; Yang, H. C.; Hong, C.-Y. Hyper-High-Sensitivity Wash-Free Magnetoreduction Assay on Biomolecules Using High-T c Superconducting Quantum Interference Devices. *J. Appl. Phys.* **2008**, *103*, 014703.
(20) Wu, K.; Su, D.; Saha, R.; Liu, J.; Chugh, V. K.; Wang, J.-P. Magnetic Particle Spectroscopy: A Short Review of Applications Using Magnetic Nanoparticles. *ACS Appl. Nano Mater.* **2020**, *3*, 4972−4989.
(21) Akiyoshi, K.; Yoshida, T.; Sasayama, T.; Elrefai, A. L.; Hara, M.; Enpuku, K. Wash-Free Detection of Biological Target Using Cluster Formation of Magnetic Markers. *J. Magn. Magn. Mater.* **2020**, *500*, 166356.
(22) Wu, K.; Chugh, V. K.; Di Girolamo, A.; Liu, J.; Saha, R.; Su, D.; Krishna, V. D.; Nair, A.; Davies, W.; Wang, Y. A.; Cheeran, M. C.-J.; Wang, J.-P. A Portable Magnetic Particle Spectrometer for Future Rapid and Wash-Free Bioassays. *ACS Appl. Mater. Interfaces* **2021**, *13*, 7966−7976.
(23) Orlov, A. V.; Znoyko, S. L.; Cherkasov, V. R.; Nikitin, M. P.; Nikitin, P. I. Multiplex Biosensing Based on Highly Sensitive Magnetic Nanolabel Quantification: Rapid Detection of Botulinum Neurotoxins A, B, and E in Liquids. *Anal. Chem.* **2016**, *88*, 10419−10426.
(24) Nikitin, M. P.; Orlov, A. V.; Znoyko, S. L.; Bragina, V. A.; Gorshkov, B. G.; Ksenevich, T. I.; Cherkasov, V. R.; Nikitin, P. I. Multiplex Biosensing with Highly Sensitive Magnetic Nanoparticle Quantification Method. *J. Magn. Magn. Mater.* **2018**, *459*, 260−264.
(25) Nikitin, M. P.; Orlov, A. V.; Sokolov, I. L.; Minakov, A. A.; Nikitin, P. I.; Ding, J.; Bader, S. D.; Rozhkova, E. A.; Novosad, V. Ultrasensitive Detection Enabled by Nonlinear Magnetization of Nanomagnetic Labels. *Nanoscale* **2018**, *10*, 11642−11650.
(26) Znoyko, S. L.; Orlov, A. V.; Pushkarev, A. V.; Mochalova, E. N.; Guteneva, N. V.; Lunin, A. V.; Nikitin, M. P.; Nikitin, P. I. Ultrasensitive Quantitative Detection of Small Molecules with Rapid Lateral-Flow Assay Based on High-Affinity Bifunctional Ligand and Magnetic Nanolabels. *Anal. Chim. Acta* **2018**, *1034*, 161−167.
(27) Khurshid, H.; Shi, Y.; Berwin, B. L.; Weaver, J. B. Evaluating Blood Clot Progression Using Magnetic Particle Spectroscopy. *Med. Phys.* **2018**, *45*, 3258−3263.
(28) Zhang, X.; Reeves, D. B.; Perreard, I. M.; Kett, W. C.; Griswold, K. E.; Gimi, B.; Weaver, J. B. Molecular Sensing with Magnetic Nanoparticles Using Magnetic Spectroscopy of Nanoparticle Brownian Motion. *Biosens. Bioelectron.* **2013**, *50*, 441−446.
(29) Graeser, M.; Knopp, T.; Grüttner, M.; Sattel, T. F.; Buzug, T. M. Analog Receive Signal Processing for Magnetic Particle Imaging. *Med. Phys.* **2013**, *40*, 042303.
(30) Pantke, D.; Holle, N.; Mogarkar, A.; Straub, M.; Schulz, V. Multifrequency Magnetic Particle Imaging Enabled by a Combined Passive and Active Drive Field Feed-through Compensation Approach. *Med. Phys.* **2019**, *46*, 4077−4086.
(31) Tay, Z. W.; Goodwill, P. W.; Hensley, D. W.; Taylor, L. A.; Zheng, B.; Conolly, S. M. A High-Throughput, Arbitrary-Waveform, Mpi Spectrometer and Relaxometer for Comprehensive Magnetic Particle Optimization and Characterization. *Sci. Rep.* **2016**, *6*, 34180.
(32) Garraud, N.; Dhavalikar, R.; Unni, M.; Savliwala, S.; Rinaldi, C.; Arnold, D. P. Benchtop Magnetic Particle Relaxometer for Detection, Characterization and Analysis of Magnetic Nanoparticles. *Phys. Med. Biol.* **2018**, *63*, 175016.
(33) Bui, T. Q.; Tew, W. L.; Woods, S. I. AC Magnetometry with Active Stabilization and Harmonic Suppression for Magnetic Nanoparticle Spectroscopy and Thermometry. *J. Appl. Phys.* **2020**, *128*, 224901.

https://doi.org/10.1021/acs.jpcc.1c05126
J. Phys. Chem. C 2021, 125, 17221−17231